

# Transitions from soft to hard piezoelectricity of (Ba, Ca)(Ti, Zr)O<sub>3</sub> ceramics via precipitation hardening

Cite as: Appl. Phys. Lett. 122, 132904 (2023); <https://doi.org/10.1063/5.0146096>

Submitted: 10 February 2023 • Accepted: 18 March 2023 • Published Online: 29 March 2023

 Mupeng Zheng,  Changhao Zhao and  Jürgen Rödel



View Online



Export Citation



CrossMark



Time to get excited.  
Lock-in Amplifiers – from DC to 8.5 GHz

[Find out more](#)

 Zurich Instruments

# Transitions from soft to hard piezoelectricity of (Ba, Ca)(Ti, Zr)O<sub>3</sub> ceramics via precipitation hardening

Cite as: Appl. Phys. Lett. **122**, 132904 (2023); doi: 10.1063/5.0146096

Submitted: 10 February 2023 · Accepted: 18 March 2023 ·

Published Online: 29 March 2023






View Online



Export Citation



CrossMark

Mupeng Zheng,<sup>1,2</sup>  Changhao Zhao,<sup>1,3,a)</sup>  and Jürgen Rödel<sup>1</sup> 

## AFFILIATIONS

<sup>1</sup>Department of Materials and Earth Sciences, Technical University of Darmstadt, Alarich-Weiss-Straße 2, Darmstadt, Germany

<sup>2</sup>Key Laboratory of Advanced Functional Materials, Ministry of Education, Faculty of Materials and Manufacturing, Beijing University of Technology, Beijing, China

<sup>3</sup>State Key Laboratory of Electrical Insulation and Power Equipment, Xi'an Jiaotong University, Xi'an, Shaanxi 710049 China

<sup>a)</sup>Author to whom correspondence should be addressed: [zhao@ceramics.tu-darmstadt.de](mailto:zhao@ceramics.tu-darmstadt.de)

## ABSTRACT

Hard piezoelectrics are essential for high-power applications, the market share of which has increased significantly over the past few years. Acceptor-doping hardening, which relies on oxygen vacancies, has been proven to be a good practice to improve mechanical quality factors. However, the high mobility of oxygen vacancies restricts the use of acceptor-doping hardening to low driving fields and temperatures. Here, we extend the design of hard-type piezoceramics via precipitation hardening and demonstrate its large potential in (Ba,Ca)(Ti,Zr)O<sub>3</sub>. A soft-to-hard transition has been realized in (Ba,Ca)(Ti,Zr)O<sub>3</sub> ceramics with an introduction of precipitates, where the mechanical quality factor and coercive field increase by over 180% and 120%, respectively. Through synchrotron x-ray diffraction and Rayleigh analysis, it is revealed that the hardening effect is attributed to the inhibition of domain wall motion by the intragranular CaTiO<sub>3</sub> precipitates. This precipitation-hardening approach offers great potential for the design of hard piezoceramics.

Published under an exclusive license by AIP Publishing. <https://doi.org/10.1063/5.0146096>

High-power applications, e.g., ultrasonic motors, actuators, transformers, and transducers, which work at resonance frequencies and large vibration velocities, are in increasing demand in many fields. The high energy losses in high-power applications can lead to severe heat generation that degrades device performance.<sup>1–3</sup> Hard piezoceramics with high mechanical quality factor ( $Q_m$ ) and low losses (mechanical and dielectric loss) are essential for these high-power applications.<sup>4–6</sup> In general, to achieve the “hardening” effect, piezoceramics are doped with lower valence cations, resulting in defect dipoles formed by acceptor substitution centers (negatively charged) and induced oxygen vacancies (positively charged) due to charge compensation.<sup>7</sup> The alignment of defect dipoles with spontaneous polarizations through defect-dipole reorientations can pin the domain walls and, thus, increase  $Q_m$ . However, hardening by defect dipoles is limited to low driving fields and low temperatures due to the mobile nature of oxygen vacancies.<sup>8,9</sup>

In analogy with metal technology,<sup>10</sup> precipitation hardening, which introduces intragranular precipitates that can directly interact with domain walls and strongly pin them, was proposed and validated

in the (Ba, Ca)TiO<sub>3</sub> (BCT) system.<sup>11</sup> It was suggested that the hardening effect in a BCT solid solution originated from the fine domains in the vicinity of intragranular precipitates, where the domain wall motion was suppressed, leading to enhanced  $Q_m$  by ~50% and slightly enhanced piezoelectric coefficient ( $d_{33}$ ). Subsequently, a more effective piezoelectric hardening via coherent plate-like precipitates has been realized in the (Li, Na)NbO<sub>3</sub> (LNN) solid solution, where the  $Q_m$  exhibits an increase by a factor of ten.<sup>12</sup>

Ba(Zr<sub>0.2</sub>Ti<sub>0.8</sub>)O<sub>3</sub>-(Ba<sub>0.7</sub>Ca<sub>0.3</sub>)TiO<sub>3</sub> (BCTZ) is an important lead-free ferroelectric material, which has attracted great interest due to its high piezoelectric properties, e.g.,  $d_{33} \sim 620$  pC/N.<sup>13</sup> It has been demonstrated that BCTZ is a promising candidate to replace the commercial ferroelectric material Pb(Zr<sub>1-x</sub>Ti<sub>x</sub>O<sub>3</sub>) (PZT).<sup>14,15</sup> Although the excellent small-signal and large-signal piezoelectric properties are comparable to those of soft PZT, BCTZ does not possess many of the functional characteristics of PZT materials. For instance, to date, no hard BCTZ materials similar to PZT-4 or PZT-8 were reported. Consequently, it is highly desired to explore the possibility of whether hard piezoelectric properties can be obtained in BCTZ piezoceramics.

Here, in this Letter, we report on excellent hard electromechanical properties achieved in the BCTZ lead-free piezoceramic via a precipitation-hardening approach. Precipitation-hardened BCTZ samples feature strongly suppressed polarization and strain but greatly enhanced  $Q_m$  and coercive field ( $E_c$ ). Succinct results on the piezoelectric hardening effect were correlated with detailed studies on the structure by synchrotron x-ray diffraction (XRD) and scanning electron microscopy. It is demonstrated that the intragranular precipitates can strongly inhibit domain wall motion, which leads to significant piezoelectric hardening effect on BCTZ piezoceramics.

$\text{Ba}_{0.83}\text{Ca}_{0.17}\text{Ti}_{0.90}\text{Zr}_{0.10}\text{O}_3$  samples were prepared by the conventional solid-state reaction method. Starting powders of  $\text{BaCO}_3$  (Alfa Aesar, 99.8%),  $\text{TiO}_2$  (Alfa Aesar, 99.9%),  $\text{CaCO}_3$  (Alfa Aesar, 99.99%), and  $\text{ZrO}_2$  (Alfa Aesar, 99.5%) were weighed according to stoichiometry and ball-milled at 250 r/min for 20 h in ethanol. After drying, the powders were calcined at 1200 °C for 4 h and ball-milled again at 250 r/min for 20 h. The calcined powders were first uniaxially pressed and then cold-isostatically pressed (with a pressure of 357 MPa) into disks with a diameter of  $\sim 10$  mm and a thickness of  $\sim 1.5$  mm. The green bodies were sintered at 1450 °C for 4 h using a tube furnace followed by air quenching. To introduce the precipitates, two-stage aging was adopted to nucleate the precipitates at the first stage (1150 °C) for 72 h and grow them at the second stage (1300 °C) for 48 h (Fig. S1 of the [supplementary material](#)).

The crystallographic phase of the samples was determined using synchrotron x-ray diffraction (XRD) at the beamline P02.1 of the Deutsches Elektronen-Synchrotron (DESY). The energy of the incident beam was 59.8 keV ( $\lambda = 0.2073$  Å). A transmission model was adopted to ensure the diffraction information is from the bulk interior. A two-dimensional (2D) detector (Dectris Pilatus3 X CdTe 2M) was used for data collection. The microstructure was characterized by scanning electron microscopy (Philips XL30 FEG). Samples were ground and polished before the measurement. The back-scattered electron (BSE) detector was used to distinguish the precipitate from the BCTZ phase.

Silver electrodes were sputtered on both the top and bottom surfaces of the samples before assessing the electrical properties. Frequency dependence of the dielectric permittivity was quantified using an impedance analyzer (Alpha-Analyzer, Novocontrol, Germany). Polarization and strain hysteresis were measured with a triangular-waveform electric field up to 3 kV/mm at 1 Hz using a Sawyer–Tower circuit equipped with an optical sensor (D63, Philtec, Inc., USA). A poling process was conducted at 4 kV/mm at 30 °C for 30 min in a silicone oil bath. After aging for 24 h, the piezoelectric charge coefficient  $d_{33}$  was determined using a commercial Berlincourt meter (Piezotest PM300, Singapore). Planar electromechanical coupling coefficient  $k_p$  and mechanical quality factor  $Q_m$  were quantified based on the impedance-frequency spectrum near the resonance frequency obtained by the impedance analyzer (Alpha-Analyzer, Novocontrol, Germany). The sub-coercive AC field dependence of permittivity was determined using the same analyzer interfaced with a high-voltage unit (HVB 300, Novocontrol, Germany).

Samples with a relative density of 95% and an average grain size of 16.5  $\mu\text{m}$  (which was determined on a statistic over 150 grains) were prepared. There were no signs of microcracking after quenching treatment. As a microcrack is an important concern, quenching of this sample geometry for the case of NBT–BT has recently been simulated

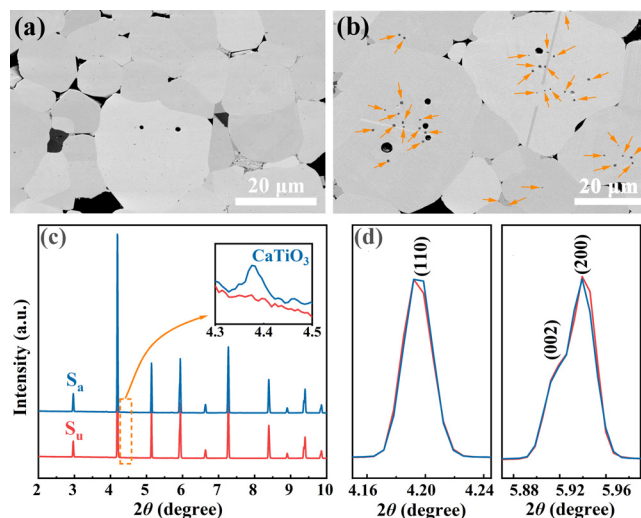


**FIG. 1.** SEM images of (a)  $S_u$  and (b)  $S_a$  samples; (c) synchrotron XRD patterns of the  $S_u$  and  $S_a$  samples; (d) magnification for the 4.20° and 5.94° diffraction peaks.

and validated with a thermal camera and quantification by elastic modulus.<sup>16</sup> As depicted in Fig. 1(a) and schematically illustrated in Fig. S1 of the [supplementary material](#), almost no secondary phase can be observed in the as-quenched sample ( $S_u$ ) from the SEM image with the BSE mode, verifying that the formation of the secondary phase was avoided by air quenching. To facilitate the generation of homogeneous precipitates, two-stage aging was adopted according to the theory of diffusional phase transitions in solids<sup>17</sup> and previous work about BCT precipitation.<sup>11</sup> The  $S_u$  samples were first-stage aged at a low temperature of 1150 °C for 72 h to form more nuclei and then second-stage aged at a high temperature of 1300 °C for 48 h to grow the precipitates. (Two-stage aged samples were denoted as  $S_a$ .) As revealed in Fig. 1(b), precipitates can be visualized by the features with lower contrast as indicated by the orange arrows. The number density of the intragranular precipitates is relatively high, while the size of the precipitates is about several hundreds of nanometers.

The synchrotron XRD patterns of the  $S_u$  and  $S_a$  samples are presented in Fig. 1(c), indicating that the  $S_u$  sample exhibits a pure perovskite phase, while a secondary phase has been traced in the  $S_a$  sample. An enlarged figure of the region in the dashed square (depicted in the inset) marks the reflections arising from the  $\text{CaTiO}_3$  (CT) phase in the  $S_a$  sample, which are absent in the  $S_u$  sample. It indicates that the CT precipitates were introduced during the aging process. The intensity and position of the 110, 002, and 200 reflections of the matrix phase (BCTZ phase) in the  $S_u$  and  $S_a$  samples are comparable except for a slight difference in the peak profiles, as depicted in Fig. 1(d). Le Bail fitting was performed to determine the lattice parameters of the matrix phase in the  $S_u$  and  $S_a$  samples using software GSAS<sup>18</sup> (Table I).

**TABLE I.** The lattice parameter comparison of the  $S_u$  and  $S_a$  samples.

Sample	$a$ (Å)	$b$ (Å)	$c$ (Å)	$c/a$	Volume (Å <sup>3</sup> )
$S_u$	3.999 11	3.999 11	4.015 64	1.004 13	64.2220
$S_a$	3.999 70	3.999 70	4.015 49	1.003 95	64.2380

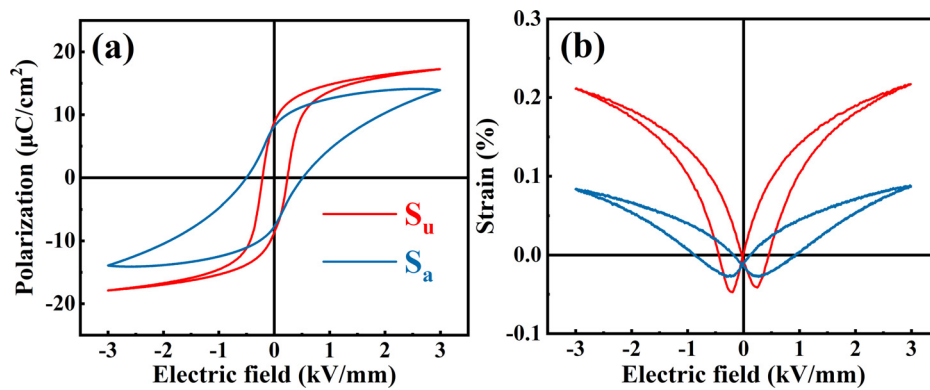


FIG. 2. Comparison of the large-signal electromechanical properties of  $S_u$  and  $S_a$  samples: (a)  $P$ - $E$  and (b)  $S$ - $E$  hysteresis loops.

Changes in the lattice parameter of the  $S_u$  and  $S_a$  samples can barely be observed, which can be attributed to the following two reasons: (a) the amount of precipitates is quite low in the  $S_a$  sample; (b) the lattice parameter of the BCTZ ceramic might be insensitive to the change in composition.

The large-signal electromechanical properties of the  $S_u$  and  $S_a$  samples by polarization and strain measurement are depicted in Figs. 2(a) and 2(b), respectively. For the  $S_a$  sample, the saturated polarization  $P_{\text{sat}}$  and the remanent polarization  $P_r$  decrease by  $\sim 20\%$  to  $13.9 \mu\text{C}/\text{cm}^2$  and by  $\sim 10\%$  to  $8.0 \mu\text{C}/\text{cm}^2$ , respectively; and the maximum strain  $S_{\text{max}}$  decreases by  $\sim 60\%$  to  $0.08\%$ . Note that the coercive field  $E_c$  of the  $S_a$  sample significantly increases by  $\sim 120\%$  (from 0.23 to 0.51 kV/mm). The small-signal electromechanical properties ( $d_{33}$ ,  $k_p$ , and  $Q_m$ ) of the  $S_u$  and  $S_a$  samples are depicted in Fig. 3. The  $S_a$  sample exhibits a  $Q_m$  enhancement from 68 to 192 ( $\sim 180\%$  enhancement) compared to the  $S_u$  sample. Notably, the increase in  $Q_m$  and  $E_c$  is the most significant characteristics of piezoelectric hardening.<sup>19</sup> Meanwhile,  $d_{33}$  and  $k_p$  of the  $S_a$  sample decreased from 395 to 190 pC/N (by  $\sim 50\%$ ) and from 0.52 to 0.28 (by  $\sim 45\%$ ), respectively, which is a common phenomenon in hardened piezoelectric materials since the domain wall contribution to piezoelectricity is suppressed.<sup>20,21</sup> The product of  $Q_m$  and  $d_{33}$  is one of the figures of merit (FOM) to evaluate piezoelectric materials for resonance applications.<sup>2</sup> As displayed in Fig. 3, the FOM of the  $S_a$  sample is found to be much higher than that of the  $S_u$

sample, indicating that the precipitation approach is an effective hardening method.

Figures 4(a) and 4(b) depict the frequency dependence of both dielectric permittivity and loss of the unpoled  $S_u$  and  $S_a$  samples. A significant increase in the low-frequency ( $10^{-2}$ – $10$  Hz) dielectric permittivity can be observed in the  $S_a$  sample, which is three times larger than the  $S_u$  sample. It is a strong indicative of the enhanced interfacial polarization (Maxwell-Wagner effect)<sup>11,22</sup> associated with an inhomogeneous dielectric medium containing more than one kind of materials with different permittivity and conductivity. The enhancement in the low-frequency permittivity in the  $S_a$  sample should be attributed to the increased interfaces between the CT precipitates and the BCTZ matrix. Interestingly, it is further observed that the dielectric permittivity of the  $S_a$  sample is smaller than that of the  $S_u$  sample at high frequencies ( $10^2$ – $10^5$  Hz), which could result from the reduced domain wall contribution.

Generally, the contribution of permittivity under weak fields can be described by the Rayleigh law as<sup>23,24</sup>

$$\varepsilon(E_0) = \varepsilon_{\text{init}} + \alpha E_0, \quad (1)$$

where  $\varepsilon(E_0)$  is the permittivity at the external electric field  $E_0$ ,  $\varepsilon_{\text{init}}$  is the initial permittivity, and  $\alpha$  is the Rayleigh coefficient. The field-amplitude-dependent permittivity and linear fittings of the permittivity-field curves with Eq. (1) are depicted in Fig. 4(c). The  $\varepsilon_{\text{init}}$  of the  $S_u$  sample

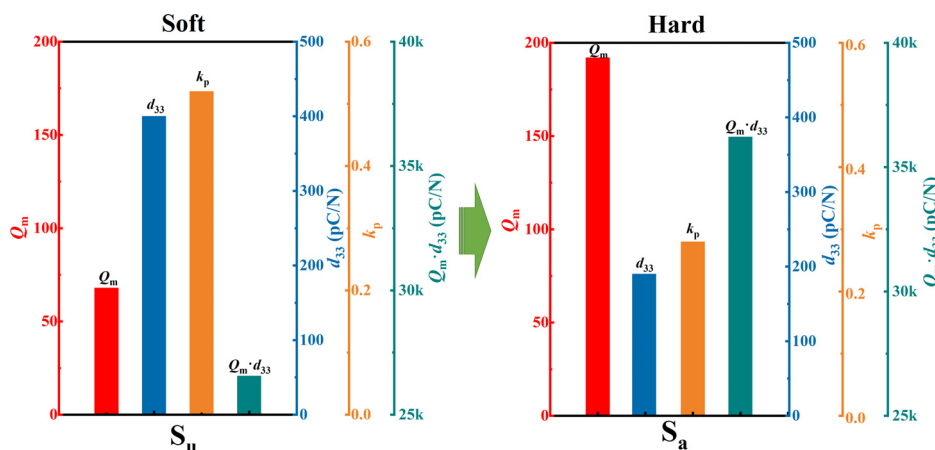
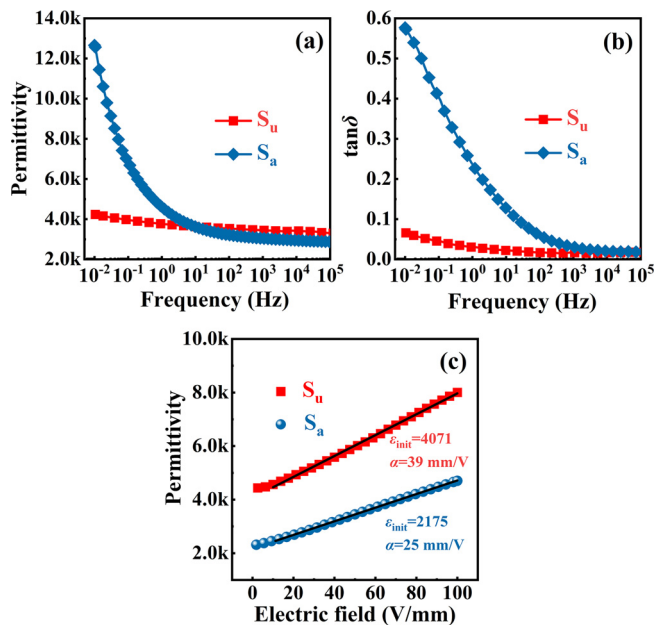


FIG. 3. Comparison of the small-signal electromechanical properties of (a)  $S_u$  and (b)  $S_a$  samples.





**FIG. 4.** Frequency-dependent (a) dielectric permittivity and (b) dielectric loss of the  $S_u$  and  $S_a$  samples; (c) subcoercive measurements of the dielectric permittivity of the  $S_u$  and  $S_a$  samples.

(4071) is much higher than that of the  $S_a$  sample (2175). Note that the  $\epsilon_{\text{ini}}$  includes both contributions from intrinsic lattice response and reversible domain wall motion.<sup>24</sup> As discussed above, there is only a slight change in the lattice parameters between  $S_u$  and  $S_a$  samples, which indicates that the intrinsic lattice contributions of the two samples should be comparable. Consequently, the largely declined  $\epsilon_{\text{ini}}$  should be caused by the decreased reversible domain wall contribution. Moreover, the  $S_a$  sample (25 mm/V) has a much smaller  $\alpha$  than the  $S_u$  sample (39 mm/V), suggesting that the irreversible domain wall motion was also strongly suppressed.

In summary, the concept of precipitation hardening was validated in soft BCTZ piezoelectric ceramics by a combination of quenching and a two-stage aging. The CT precipitates are demonstrated to have a profound impact on both the small-signal and large-signal electromechanical properties of the ceramics, leading to an enhancement of  $Q_m$  by 180% and  $E_c$  by 120%. The hardening mechanism is attributed to the strong restriction to domain wall motion caused by intragranular precipitates.

See the [supplementary material](#) for the temperature profile of the precipitate-formation process.

This work was supported by Deutsche Forschungsgemeinschaft (Grant No. 462460745) and the Beijing Natural Science Foundation (Grant No. J123004). M.Z. acknowledges the financial support from the China Scholarship Council.

## AUTHOR DECLARATIONS

### Conflict of Interest

The authors have no conflicts to disclose.

### Author Contributions

**Mupeng Zheng:** Data curation (equal); Formal analysis (equal); Investigation (equal); Visualization (equal); Writing – original draft (equal). **Changhao Zhao:** Data curation (equal); Formal analysis (equal); Investigation (equal); Writing – review & editing (equal). **Jürgen Rödel:** Data curation (equal); Funding acquisition (lead); Project administration (lead); Writing – review & editing (equal).

## DATA AVAILABILITY

The data that support the findings of this study are available from the corresponding author upon reasonable request.

## REFERENCES

- <sup>1</sup>L. Chen, H. Liu, H. Qi, and J. Chen, *Prog. Mater. Sci.* **127**, 100944 (2022).
- <sup>2</sup>K. Uchino, *Ferroelectric Devices*, 2nd ed. (CRC Press, 2010).
- <sup>3</sup>J. Rödel, K. G. Webber, R. Dittmer, W. Jo, M. Kimura, and D. Damjanovic, *J. Eur. Ceram. Soc.* **35**(6), 1659 (2015).
- <sup>4</sup>G. Liu, S. J. Zhang, W. H. Jiang, and W. W. Cao, *Mater. Sci. Eng. R.* **89**, 1 (2015).
- <sup>5</sup>K. Uchino, J. Zheng, A. Joshi, Y.-H. Chen, S. Yoshikawa, S. Hirose, S. Takahashi, and J. W. C. de Vries, *J. Electroceram.* **2**(1), 33 (1998).
- <sup>6</sup>T. Tayama, Y. Takagi, and H. Nagata, *J. Appl. Phys.* **132**(6), 064101 (2022).
- <sup>7</sup>K. Uchino, *High-Power Piezoelectrics and Loss Mechanisms* (CRC Press, New York, 2020).
- <sup>8</sup>K. Uchino, J. H. Zheng, Y. H. Chen, X. H. Du, J. Ryu, Y. Gao, S. Ural, S. Priya, and S. Hirose, *J. Mater. Sci.* **41**(1), 217 (2006).
- <sup>9</sup>Y. Doshida, H. Shimizu, Y. Mizuno, and H. Tamura, *Jpn. J. Appl. Phys.* **52**(7S), 07HE01 (2013).
- <sup>10</sup>A. J. Ardell, *Metall. Trans. A* **16**(12), 2131 (1985).
- <sup>11</sup>C. Zhao, S. Gao, T. Yang, M. Scherer, J. Schultheiss, D. Meier, X. Tan, H.-J. Kleebe, L.-Q. Chen, J. Koruza, and J. Rödel, *Adv. Mater.* **33**(36), 2102421 (2021).
- <sup>12</sup>C. Zhao, S. Gao, H.-J. Kleebe, X. Tan, J. Koruza, and J. Rödel, *Adv. Mater.* **34**(38), 2202379 (2022).
- <sup>13</sup>W. F. Liu and X. B. Ren, *Phys. Rev. Lett.* **103**(25), 257602 (2009).
- <sup>14</sup>X. Yan, M. Zheng, X. Gao, M. Zhu, and Y. Hou, *J. Mater. Chem. C* **8**(39), 13530 (2020).
- <sup>15</sup>Y. Zhang, H. Sun, and W. Chen, *J. Phys. Chem. Solids* **114**, 207 (2018).
- <sup>16</sup>M.-H. Zhang, P. Breckner, T. Froemling, J. Rödel, and K. V. Lalitha, *Appl. Phys. Lett.* **116**, 262902 (2020).
- <sup>17</sup>D. A. Porter, K. E. Easterling, and K. E. Easterling, *Phase Transformations in Metals and Alloys* (revised reprint), 3rd ed. (CRC Press, 2009).
- <sup>18</sup>A. Le Bail, *Powder Diff.* **20**(4), 316 (2005).
- <sup>19</sup>Y.-X. Liu, W. Qu, H.-C. Thong, Y. Zhang, Y. Zhang, F.-Z. Yao, T. N. Nguyen, J.-W. Li, M.-H. Zhang, J.-F. Li, B. Han, W. Gong, H. Wu, C. Wu, B. Xu, and K. Wang, *Adv. Mater.* **34**(29), 2202558 (2022).
- <sup>20</sup>Y. Yan, K.-H. Cho, and S. Priya, *J. Am. Ceram. Soc.* **94**(11), 3953 (2011).
- <sup>21</sup>B. H. Watson III, M. J. Brova, M. A. Fanton, R. J. Meyer, Jr., and G. L. Messing, *J. Am. Ceram. Soc.* **103**(11), 6319 (2020).
- <sup>22</sup>C. C. Wang, Y. J. Yan, L. W. Zhang, M. Y. Cui, G. L. Xie, and B. S. Cao, *Scr. Mater.* **54**(8), 1501 (2006).
- <sup>23</sup>D. A. Hall, *J. Mater. Sci.* **36**(19), 4575 (2001).
- <sup>24</sup>D. Damjanovic and M. Demartin, *J. Phys. D: Appl. Phys.* **29**(7), 2057 (1996).